Coupling Phenomena in Concentric Multi-Applicator Phased Array Hyperthermia Systems

Konstantina S. Nikita and Nikolaos K. Uzunoglu, *Member, IEEE*

Abstract—**The coupling between the waveguide applicators of a four-element phased array hyperthermia system irradiating a three-layered cylindrical tissue model of circular cross section is analyzed theoretically. The fields inside the tissue layers are expressed in terms of cylindrical vector wave functions satisfying the corresponding wave equations, while the fields inside each waveguide are expanded in terms of guided and evanescent normal modes. Then, by implementing the appropriate boundary conditions, a system of four coupled integral equations is derived in terms of the unknown electric field distributions on the open waveguide apertures. This system is solved by expanding the unknown electric field on each aperture into waveguide normal modes and by applying a Galerkin's procedure. The self reflection coefficient and the mutual coupling coefficients are then determined and numerical results for a four-element phased array hyperthermia system are computed and presented for different waveguide applicator sizes and settings.**

I. Introduction

HYPERTHERMIA FOR DEEP-SEATED tumors is a technically difficult problem because of the limited penetration of both electromagnetic and ultrasound radiation used to deliver energy to the tumor. Phased array principles have been proposed in [1] and [2] in the past and are being employed in [3]–[6] by several researchers in order to enhance penetration depth from body's surface. In contrast to phased array employed in radar systems, it is the near field radiated from each applicator that is important in a phased array hyperthermia system. A major advantage of coherent radiating multi-element heating systems consisting of waveguides or multiple dipole antennas is that they provide the possibility of controlling the electromagnetic energy deposited in the tissue and optimizing the heating for any given body model by phase and amplitude adjustment. Researchers approached this optimization problem in various ways [8]–[11], but in all the works involving computation of electromagnetic field distribution produced inside tissues by phased array hyperthermia systems, coupling between system elements was neglected [8]–[13].

In a multi-element system, the influence on the radiation of each element resulting from the other elements of the system is a significant reason for nonpredictable behavior of this type of systems. For some configurations the waves coupled to an individual element from the other radiating elements may be strong and add vectorially, producing a wave travelling toward the generator of this element that appears to be a large reflection. The recently gathered clinical experience in using phased array hyperthermia systems and phantom studies [14]–[16] substantiated the above points and showed that coupling can produce potentially major effects on SAR distributions.

The experience with the first generation annular phased array system (APA or BSD 1000) [5] consisting of dielectrically loaded horn antennas radiating into the same chamber and driven by a single power source was that a significant interaction between radiators is normally observed. In addition, the evaluation of the Sigma 60 applicator of the BSD 2000 system, consisting of four pairs of dipole antennas electrically isolated with independent phase and amplitude control of each pair [17] showed that coupling effects can occur and can even produce SAR patterns which are steered in the opposite direction from what would have occurred in the absence of coupling. Phantom measurements with the four-waveguide system [16] which uses an isolating type of feed to distribute power to the individual applicators, indicated that significant coupling between elements still occurs via the radiating apertures.

In the present work, the coupling between the waveguide applicators of a phased array hyperthermia system radiating into a three-layered cylindrical body model of circular cross section is treated semianalytically. The motivation of pursuing this work is the practical use of phased array systems using waveguide applicators in hyperthermia. Radiation from flanged rectangular open-aperture waveguides into a stratified medium has been analyzed by several authors [18]–[20]. The absorbed power distribution from multiple waveguide applicators has been treated in a two-dimensional problem [20] by employing a numerical solution of the coupled integral equations based on the method of moments, without taking into account coupling phenomena between applicators. The necessity of more complete knowledge of the SAR distribution for optimal control and pretreatment planning in order to use the phased array systems effectively, provided the rationale for analyzing in detail the behavior of these systems by taking into account the modification of each aperture field resulting from the other radiating elements of the system. The fact that the exact mechanism of interaction between system elements is important when designing and operating a multiport microwave device, such as a phased array hyperthermia system, was also one of the reasons for treating this boundary value problem theoretically.

In this paper, coupling phenomena occurred in a phased array hyperthermia system using four water-loaded rectangular

Manuscript received December 31, 1994; revised October 2, 1995.

The authors are with the National Technical University of Athens, Department of Electrical and Computer Engineering, Athens 10682, Greece.

Publisher Item Identifier: S 0018-9480(96)00478-4.

aperture 5.8×2.9 cm^2 waveguide applicators, are studied, by using the scattering matrix notation. The excitation (phase and amplitude) of each applicator can be controlled independently and the four element phased array hyperthermia system can be described as a four port electromagnetic device. Therefore the scattering matrix is a 4×4 matrix with complex elements S_{ij} $(i = 1,2,3,4;\ j = 1,2,3,4)$, which will be referred to as the $\underline{S}$ matrix. Furthermore, the use of four waveguide applicators with larger aperture (15×10 cm^2) is investigated and the scattering parameters at the operation range of this system are computed.

In the following analysis an $\exp(+j\omega t)$ time dependence is assumed for the field quantities and it is suppressed throughout the analysis.

II. Formulation of the Boundary Value Problem

The phased array hyperthermia system examined in this paper consists of four identical rectangular waveguide applicators. The geometry of the radiating system looking into a three layered cylindrical body model of circular cross section is shown in Fig. 1. The three layers correspond to skin, fat, and muscle tissues. The electromagnetic properties of the layers are denoted with the corresponding relative complex permittivities $\varepsilon_1, \varepsilon_2, \varepsilon_3$ and relative magnetic permeabilities μ_1, μ_2 and μ_3 although in practice in tissue media $\mu_1 = \mu_2 = \mu_3 = 1$. The free-space wavenumber is $k_0 = \omega\sqrt{\varepsilon_0\mu_0}$, where ε_0 and μ_0 are the free-space permittivity and permeability, respectively. The applicators are filled with a dielectric material of relative permittivity ε_w and relative permeability μ_w and have an aperture size of $a \times b$ $(b < a)$. It is assumed that apertures are not completely planar and placed at body's periphery with the large dimension at the transverse direction circulating around the cylindrical body's surface and the small dimension parallel to the cylindrical body's axis. Thus the entire aperture of each applicator is assumed to be in direct contact with the body's surface. Radiating apertures are separated by perfectly conducting flanges. By considering a global cylindrical polar coordinate system ρ, φ, z the position vector of the ℓth applicator's aperture center is expressed $\underline{r}_{0\ell} = \rho_3\hat{\rho} + \varphi_{0\ell}\hat{\varphi} + (b/2)\hat{z}$, $\ell = 1,2,3,4$.

A. Electromagnetic Fields Inside the Tissue Layers

The solution of the wave equation

$$(\nabla \times \nabla \times -k_0^2\varepsilon_i\mu_i)\underline{E}_i(\underline{r}) = 0 \tag{1}$$

in cylindrical polar coordinates, inside the three regions $i = 1,2,3$ is expressed in terms of cylindrical vector wave functions [21]. Thus

$$\underline{E}_i(\underline{r}) = \int_{-\infty}^{+\infty} dk \sum_{m=-\infty}^{m=+\infty} \left(a_{im}\underline{M}^{(1)}_{m,k}(\underline{r}, k_i) + b_{im}\underline{N}^{(1)}_{m,k}(\underline{r}, k_i) + a'_{im}\underline{M}^{(2)}_{m,k}(\underline{r}, k_i) + b'_{im}\underline{N}^{(2)}_{m,k}(\underline{r}, k_i)\right) \tag{2}$$

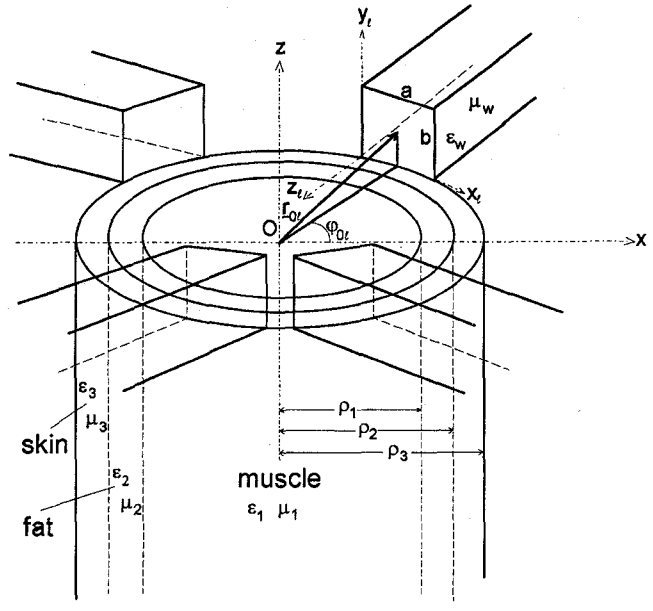

Fig. 1. Three-layered cylindrical body model of circular cross section irradiated by four rectangular waveguide hyperthermia applicators.

where

$k_i = k_0\sqrt{\varepsilon_i}$ and

$a_{im}, b_{im}, a_{im}, b_{im}$ are unknown coefficients to be determined.

The cylindrical vector wave functions $\underline{M}^{(q)}_{m,k}(\underline{r}, k_i)$, $\underline{N}^{(q)}_{m,k}(\underline{r}, k_i)$ are given by the following equations

$$\underline{M}^{(q)}_{m,k}(\underline{r}, k_i) = \nabla \times \left(\hat{z}e^{jm\varphi}e^{jkz}Z^{(q)}_m(\alpha_i, \rho)\right) \tag{3a}$$

$$\underline{N}^{(q)}_{m,k}(\underline{r}, k_i) = \frac{1}{k_i}\nabla \times \underline{M}^{(q)}_{m,k}(\underline{r}, k_i), \quad q = 1,2 \tag{3b}$$

where the ρ, φ and z cylindrical polar coordinates are shown in Fig. 1

$$\alpha_i = (k_i^2 - k^2)^{1/2} \tag{4}$$

and $Z^{(q)}_m(\alpha_i\rho)$ is the solution of Bessel's equation

$$\frac{1}{\rho}\frac{\partial}{\partial\rho}\left(\rho\frac{\partial Z^{(q)}_m(\alpha_i\rho)}{\partial\rho}\right) + \left(\alpha_i^2 - \frac{m^2}{\rho^2}\right)Z^{(q)}_m(\alpha_i\rho) = 0 \tag{5}$$

being Bessel's or Neuman's function for $q = 1$ or 2, respectively, thus

$$Z^{(1)}_m(\alpha_i\rho) = J_m(\alpha_i\rho) \quad \text{and} \quad Z^{(2)}_m(\alpha_i\rho) = Y_m(\alpha_i\rho). \tag{6}$$

The corresponding magnetic field inside the ith layer can be computed easily by employing the Maxwell-Faraday equation, leading to the expression

$$\underline{H}_i(\underline{r}) = \frac{jk_i}{\omega\mu_0\mu_i}\int_{-\infty}^{+\infty} dk \sum_{m=-\infty}^{m=+\infty} \left(a_{im}\underline{N}^{(1)}_{m,k}(\underline{r}, k_i) + b_{im}\underline{M}^{(1)}_{m,k}(\underline{r}, k_i) + a'_{im}\underline{N}^{(2)}_{m,k}(\underline{r}, k_i) + b'_{im}\underline{M}^{(2)}_{m,k}(\underline{r}, k_i)\right) \tag{7}$$

with $i = 1,2,3$.

Inside the $i = 2$ and 3 (skin and fat) layers, respectively, both $J_m(\alpha_i\rho)$ and $Y_m(\alpha_i\rho)$ solutions are encountered in contrast to the $i = 1$ (muscle) layer, where it is required that

$$a'_{1m} = b'_{1m} = 0 \tag{8}$$

subject to the condition that electric field must be of finite value, when $\rho \to 0$.

On satisfying the continuity of the tangential (φ and z) electric and magnetic field components on the $\rho = \rho_1$ (muscle-fat) and $\rho = \rho_2$ (fat-skin) interfaces, a system of two equations is obtained on each interface for φ and z components independently. Then by eliminating the $a_{1m}(b_{1m})$ coefficient, the amplitudes a^1_{2m}, b^1_{2m} in (2) can be expressed in terms of the amplitudes a_{2m}, b_{2m}. At the end of this procedure the following relation is obtained

$$\underline{c}'_{2m} = \underline{\bar{R}}_{2m}\underline{c}_{2m} \tag{9}$$

where

$$\underline{c}_{2m} = a_{2m}\hat{\varphi} + b_{2m}\hat{z}$$
$$\underline{c}'_{2m} = a_{2m},\hat{\varphi} + b_{2m},\hat{z}$$

are tangential vector coefficients, and

$$\underline{\bar{R}}_{2m} = \frac{J_m(\alpha_2\rho)}{Y_m(\alpha_2\rho)}\left(\underline{\bar{T}}^{(2)}_{2m} - \frac{k_1}{k_2}\underline{\bar{T}}^{(1)}_{1m}\left(\underline{\bar{D}}^{(1)}_{1m}\right)^{-1}\underline{\bar{D}}^{(2)}_{2m}\right)^{-1} \times \left(\frac{k_1}{k_2}\underline{\bar{T}}^{(1)}_{1m}\left(\underline{\bar{D}}^{(1)}_{1m}\right)^{-1}\underline{\bar{D}}^{(1)}_{2m} - \underline{\bar{T}}^{(1)}_{2m}\right)^{-1} \text{ at } \rho = \rho_1 \tag{10}$$

$$\underline{\bar{D}}^{(q)}_{im}(k;\rho) = \begin{pmatrix} -\frac{\partial Z^{(q)}_m(\alpha_i\rho)/\partial\rho}{Z^{(q)}_m(\alpha_i\rho)} & -\frac{mk}{k_i\rho} \\ 0 & \frac{\alpha_i^2}{k_i} \end{pmatrix} \tag{11}$$

$$\underline{\bar{T}}^{(q)}_{im}(k;\rho) = \begin{pmatrix} -\frac{mk}{k_i\rho} & -\frac{\partial Z^{(q)}_m(\alpha_i\rho)/\partial\rho}{Z^{(q)}_m(\alpha_i\rho)} \\ \frac{\alpha_i^2}{k_i} & 0 \end{pmatrix} \tag{12}$$

where $i = 1, 2$ and $Z^{(q)}_m$ $(\alpha_i\rho)$ are given by (6) with $q = 1, 2$.

In the same manner by imposing the boundary conditions on the $\rho = \rho_2$ skin-fat layers' interface and then eliminating the $\underline{c}'_{2m}$, $\underline{c}_{2m}$ vector coefficients, the following relation is obtained between the $\underline{c}'_{3m}$, $\underline{c}_{3m}$ tangential vectors

$$\underline{c}'_{3m} = \underline{\bar{R}}_{3m}\underline{c}_{3m} \tag{13}$$

where

$$\underline{c}_{3m} = a_{3m}\hat{\varphi} + b_{3m}\hat{z}$$
$$\underline{c}'_{3m} = a'_{3m}\hat{\varphi} + b'_{3m}\hat{z}$$
$$\underline{\bar{R}}_{3m} = \frac{J_m(\alpha_3\rho)}{Y_m(\alpha_3\rho)}\left(\underline{\bar{T}}^{(2)}_{3m} - \frac{k_2}{k_3}\underline{\bar{G}}_{2m}\underline{\bar{F}}_{2m}\underline{\bar{D}}^{(2)}_{3m}\right)^{-1} \times \left(-\underline{\bar{T}}^{(1)}_{3m} + \frac{k_2}{k_3}\underline{\bar{G}}_{2m}\underline{\bar{F}}_{2m}\underline{\bar{D}}^{(1)}_{3m}\right)^{-1} \text{ at } \rho = \rho_2 \tag{14}$$

where $\underline{\bar{D}}^{(q)}_{3m}, \underline{\bar{T}}^{(q)}_{3m}$ are obtained by setting $i = 3$ in (11) and (12), respectively, and

$$\underline{\bar{G}}_{2m}(k;\rho) = \underline{\bar{T}}^{(1)}_{2m} + \frac{Y_m(\alpha_2\rho)}{J_m(\alpha_2\rho)}\underline{\bar{T}}^{(2)}_{2m}\underline{\bar{R}}_{2m} \tag{15}$$

$$\underline{\bar{F}}_{2m}(k;\rho) = \left[\underline{\bar{D}}^{(1)}_{2m} + \frac{Y_m(\alpha_2\rho)}{J_m(\alpha_2\rho)}\underline{\bar{D}}^{(2)}_{2m}\underline{\bar{R}}_{2m}\right]^{-1}. \tag{16}$$

Substituting (13) into (2) for $i = 3$, the electric field inside the skin layer is obtained in the following form

$$\underline{E}_{3,t}(\underline{r}) = \int_{-\infty}^{+\infty} dk \sum_{m=-\infty}^{m=+\infty} (e^{jm\varphi}e^{jkz}J_m(\alpha_3\rho)\underline{\bar{L}}(m,k;\rho)\underline{c}_{3m}) \tag{17}$$

with $\rho_2 < \rho < \rho_3$, the subscript t denoting the tangential character of the electric field and

$$\underline{\bar{L}}(m,k;\rho) = \underline{\bar{D}}^{(1)}_{3m} + \frac{Y_m(\alpha_3\rho)}{J_m(\alpha_3\rho)}\underline{\bar{D}}^{(2)}_{3m}\underline{\bar{R}}_{3m}. \tag{18}$$

B. Electromagnetic Fields Inside the Waveguide Applicators

The normal modes satisfying the boundary conditions on the sidewalls of the rectangular waveguide are well known [22]. In order to achieve in practice a stable operation of the waveguide applicator and a good match to a power generator, it is desirable to have only a single propagating mode. This means that only the TE_{10} mode cutoff frequency must be less than the operating frequency, while an infinite number of evanescent modes are present only near the discontinuity regions, such as the open apertures of the rectangular waveguides (see Fig. 1). Therefore the fields inside each waveguide can be described as the superposition of the incident TE_{10} mode and an infinite number of all the reflected modes. Following the notation of [22], the transverse electric field inside the ℓth waveguide applicator ($\ell = 1, 2, 3, 4$) can be written, with respect to the local cartesian coordinates system x_ℓ, y_ℓ, z_ℓ (see Fig. 1), as follows

$$\underline{E}^w_{\ell,t}(x_\ell, y_\ell, z_\ell) = A_{\ell,1}\underline{e}^{\mathrm{TE}}_{1,t}(x_\ell, y_\ell)\frac{j\omega\mu_0\mu_w}{u_1}e^{-j\gamma_1 z_\ell} + \sum_{n=1}^{\infty}\left(A'_{\ell,n}\underline{e}^{\mathrm{TE}}_{n,t}(x_\ell, y_\ell)\frac{j\omega\mu_0\mu_w}{u_n}e^{j\gamma_n z_\ell} + B'_{\ell,n}\underline{e}^{\mathrm{TM}}_{n,t}(x_\ell, y_\ell)\left(-\frac{j\lambda_n}{v_n}\right)e^{j\lambda_n z_\ell}\right) \tag{19}$$

where the subscript t is used to denote the transverse field components, $A_{1,\ell}$ is the complex amplitude of the excited TE_{10} mode in the $\ell$the waveguide, $A'_{\ell,n}$ and $B'_{\ell,n}$ are the complex amplitudes of the reflected transverse electric fields of the nth TE and nth TM modes, respectively, in the ℓth waveguide and γ_n, λ_n are propagation constants of TE and TM modes, respectively

$$\gamma_n = \left(k_0^2\varepsilon_w\mu_w - u_n^2\right)^{1/2} \tag{20a}$$

$$\lambda_n = \left(k_0^2\varepsilon_w\mu_w - v_n^2\right)^{1/2}. \tag{20b}$$

The transverse $\underline{e}^{\mathrm{TE}}_{n,t}$ and $\underline{e}^{\mathrm{TM}}_{n,t}$ modal fields are [22]

$$\underline{e}^{\mathrm{TE}}_{n,t}(x_\ell, y_\ell) = (\hat{z}_\ell \times \nabla_{\ell,t}\psi_n)/u_n \quad \underline{e}^{\mathrm{TM}}_{n,t}(x_\ell, y_\ell) = \nabla_{\ell,t}\phi_n/v_n \tag{21}$$

with $\nabla_{\ell,t}(\partial/\partial x_\ell\hat{x}_\ell + \partial/\partial y_\ell\hat{y}_\ell)$. The scalar functions ψ_n and ϕ_n satisfy the wave equations

$$\left(\nabla^2 + u_n^2\right)\psi_n = 0 \quad \left(\nabla^2 + v_n^2\right)\phi_n = 0 \tag{22}$$

and the boundary conditions

$$\partial\psi_n/\partial n_\ell = 0 \quad \phi_n = 0 \tag{23}$$

on the walls of the waveguide, with $\partial/\partial n_\ell$ being the normal derivative.

The orthogonal properties of this representation [22] are

$$\iint_{\Gamma_\ell} \underline{e}_{n,t}^{\mathrm{TE}} \cdot \underline{e}_{p,t}^{\mathrm{TE}} d\Gamma_\ell = \iint_{\Gamma_\ell} \underline{e}_{n,t}^{\mathrm{TM}} \cdot \underline{e}_{p,t}^{\mathrm{TM}} d\Gamma_\ell = \delta_{np} \quad (24)$$

$$\iint_{\Gamma_\ell} \underline{e}_{n,t}^{\mathrm{TE}} \cdot \underline{e}_{p,t}^{\mathrm{TM}} d\Gamma_\ell = 0 \quad (25)$$

where Γ_ℓ is an arbitrary cross section of the ℓth applicator and δ_{np} is Kronecker's delta. The magnetic fields associated with the $\underline{e}_{n,t}^{\mathrm{TE}}$ and $\underline{e}_{n,t}^{\mathrm{TM}}$ fields can be written as follows [22]

$$\underline{h}_{n,t}^{\mathrm{TE}}(x_\ell, y_\ell) = -\frac{1}{u_n} \nabla_{\ell,t} \psi_n \quad \underline{h}_{n,t}^{\mathrm{TM}}(x_\ell, y_\ell) = \hat{z}_\ell \times \nabla_{\ell,t} \phi_n. \quad (26)$$

The magnetic field inside the ℓth applicator can be derived by applying Maxwell-Faraday equation to the expression (19) for the corresponding electric field.

C. Integral Equation on the $\rho = \rho_3$ Body's Surface

In order to satisfy the continuity of the electric and magnetic field components on the $\rho = \rho_3$ contact surface between cylindrical body model and radiating apertures, an unknown electric field $\underline{E}_a(\varphi, z)$ is defined. Then on the cylindrical surface $\rho = \rho_3$ it is required that

$$\underline{E}_a(\varphi, z) = \begin{cases} \underline{E}_{1,t}^w(x_1, y_1, z_1 = 0), & \text{in aperture } \Gamma_1 \\ \underline{E}_{2,t}^w(x_2, y_2, z_2 = 0), & \text{in aperture } \Gamma_2 \\ \underline{E}_{3,t}^w(x_3, y_3, z_3 = 0), & \text{in aperture } \Gamma_3 \\ \underline{E}_{4,t}^w(x_4, y_4, z_4 = 0), & \text{in aperture } \Gamma_4 \\ 0, & \text{anywhere else} \end{cases} \quad (27)$$

where the relations between the coordinates x_ℓ, y_ℓ with respect to the ℓth applicator's corner attached local cartesian coordinates system and the coordinates φ, z with respect to the global cylindrical polar coordinates system are given by the following equations

$$x_\ell = \rho_3(\varphi_{0\ell} + a/(2\rho_3) - \varphi), \quad y_\ell = z \text{ with } \ell = 1, 2, 3, 4. \quad (28)$$

The unknown aperture field must also satisfy the following relation

$$\underline{E}_a(\varphi, z) = \underline{E}_{3,t}(\rho = \rho_3, \varphi, z). \quad (29)$$

Note that $\underline{E}_{3,t}$ and $\underline{E}_{\ell t}^w$ ($\ell = 1, 2, 3, 4$) fields have already been expressed in (17) and (19) respectively in terms of unknown coefficients $\underline{c}_{3m}$ and $A'_{\ell,n}, B'_{\ell,n}$ ($\ell = 1, 2, 3, 4$). These coefficients can be expressed in terms of the aperture function $\underline{E}_a(\varphi, z)$ which is also an unknown quantity. Considering (27) and (29), by employing the orthogonal properties given in (24) and (25) for the transverse $\underline{e}_{n,t}^{\mathrm{TE}}$ and $\underline{e}_{n,t}^{\mathrm{TM}}$ modal fields, the following expressions are obtained

$$\underline{c}_{3m}(k) = \frac{1}{(2\pi)^2} \frac{1}{J_m(\alpha_3 \rho_3)} (\underline{\bar{L}}(m, k; \rho_3))^{-1} \times \int_0^{2\pi} \int_{-\infty}^{+\infty} d\varphi\, dz\, e^{-\jmath m\varphi} e^{-\jmath kz} \underline{E}_a(\varphi, z) \quad (30)$$

$$A_{\ell,1}\delta_{n1} + A'_{\ell,n} = \frac{u_n}{j\omega\mu_0\mu_w} \iint_{\Gamma_\ell} \rho_3 d\varphi\, dz \underline{E}_a(\varphi, z) \cdot \underline{e}_{n,t}^{\mathrm{TE}} \quad (31)$$

$$B'_{\ell,n} = \frac{v_n}{j\lambda_n} \iint_{\Gamma_\ell} \rho_3 d\varphi\, dz \underline{E}_a(\varphi, z) \cdot \underline{e}_{n,t}^{\mathrm{TM}}. \quad (32)$$

The final step in obtaining the system of integral equations, is to satisfy the continuity of the tangential magnetic fields on the $\rho = \rho_3$ surface. By substituting (30), (31), and (32) into this boundary condition, the following system of coupled integral equations is obtained

$$\sum_{q=1}^{4} \iint_{\Gamma_\ell} \rho_3 d\varphi'\, dz' \underline{\bar{K}}_{\ell q}(\varphi, z/\varphi, z') \underline{E}_a(\varphi, z') = 2A_{\ell,1} \underline{h}_{1,t}^{\mathrm{TE}}\left(\frac{j\gamma_1}{u_1}\right) \quad \ell = 1, 2, 3, 4 \quad (33)$$

where

$$\underline{h}_{1,t}^{\mathrm{TE}} = -\frac{1}{u_1} \nabla_{\ell,t} \psi_1 \quad (34)$$

is the incident TE_{10} mode transverse magnetic field on the aperture of the ℓth waveguide applicator, and the kernel matrices $\underline{\bar{K}}_{\ell q}(\varphi, z/\varphi', z')$, $q = 1, \ldots, 4/\ell = 1, \ldots, 4$ indicate the effect of coupling from the qth aperture $(\varphi', z') \in \Gamma_q$ to the ℓth aperture $(\varphi, z) \in \Gamma_\ell$. The above set of integral equations can be modified in terms of local cartesian coordinates x, y with respect to the ℓth aperture's corner attached local cartesian coordinates system (x_ℓ, y_ℓ, z_ℓ) and x', y' with respect to the qth aperture's corner attached local cartesian coordinates system (x_q, y_q, z_q) by using (28). Thus the system of integral equations (33) can be expressed in the following form

$$\sum_{q=1}^{4} \iint_{\Gamma_q} dx'\, dy' \underline{\bar{K}}_{\ell q}(x, y/x', y') \underline{E}_a(x', y') = 2A_{\ell,1} \underline{h}_{1,t}^{\mathrm{TE}}\left(\frac{j\gamma_1}{u_1}\right) \quad \ell = 1, 2, 3, 4 \quad (35)$$

where the kernel matrix functions $\underline{\bar{K}}_{\ell q}(x, y/x', y')$ are given in the Appendix.

III. Solution of the Coupled Integral Equations

In order to determine the electric field distribution on the waveguide apertures and then the scattering parameters of the system (i.e., the self reflected TE_{10} mode amplitude on the excited aperture, and the coupled TE_{10} amplitudes to the other three apertures), the system of integral equations (35) was solved. To this end a Galerkin's technique was adopted by expanding the unknown transverse electric field on each aperture $\underline{E}_{q,a}$ into waveguide normal modes. Therefore, with respect to the qth ($q = 1, 2, 3, 4$) aperture's corner attached local cartesian coordinate system, the electric field on the same aperture is expressed in the following form

$$\underline{E}_{q,a} = \sum_{n=1}^{\infty} \left(g_{q,n} \underline{e}_{n,t}^{\mathrm{TE}} + f_{q,n} \underline{e}_{n,t}^{\mathrm{TM}}\right) \quad q = 1, 2, 3, 4. \quad (36)$$

By substituting (36) into the system of coupled integral (35), taking the inner products of both sides of each equation ($\ell = 1, 2, 3, 4$) with $\underline{h}_{p,t}^{\mathrm{TE}}$ and $\underline{h}_{p,t}^{\mathrm{TM}}$, the magnetic vectors of the

TE and TM modes of the ℓth waveguide, and then integrating over the ℓth waveguide aperture Γ_ℓ, the system of integral equations (35) is converted into an infinite system of linear equations of the following type as in (37) shown at the bottom of the page, where

$$\begin{pmatrix} K^{\ell q}_{pn,\mathrm{EE}} \\ K^{\ell q}_{pn,\mathrm{EM}} \\ K^{\ell q}_{pn,\mathrm{ME}} \\ K^{\ell q}_{pn,\mathrm{MM}} \end{pmatrix} = \int\!\!\int_{\Gamma_\ell} dx\,dy \int\!\!\int_{\Gamma_q} dx'\,dy' \begin{pmatrix} \underline{h}^{\mathrm{TE}}_{p,t}(x,y) \\ \underline{h}^{\mathrm{TE}}_{p,t}(x,y) \\ \underline{h}^{\mathrm{TM}}_{p,t}(x,y) \\ \underline{h}^{\mathrm{TM}}_{p,t}(x,y) \end{pmatrix} \cdot \underline{\bar{K}}_{\ell q}(x,y/x',y') \cdot \begin{pmatrix} \underline{e}^{\mathrm{TE}}_{n,t}(x',y') \\ \underline{e}^{\mathrm{TM}}_{n,t}(x',y') \\ \underline{e}^{\mathrm{TE}}_{n,t}(x',y') \\ \underline{e}^{\mathrm{TM}}_{n,t}(x',y') \end{pmatrix}. \quad (38)$$

In computing the numerical values of the matrix elements $K^{\ell q}_{pn,\mathrm{EE}}, K^{\ell q}_{pn,\mathrm{EM}}, K^{\ell q}_{pn,\mathrm{ME}}$ and $K^{\ell q}_{pn,\mathrm{MM}}$, the expression for the $\underline{\bar{K}}_{\ell q}$ matrices given in the Appendix is employed. In the self waveguide matrices $\underline{\bar{K}}_{\ell q}$ $(\ell = q)$, diagonal matrix elements $(n = p)$ are obtained due to waveguide mode contributions to these matrices. The stratified layer contribution to $\underline{\bar{K}}_{\ell q}$ matrices is expressed through the Fourier transformations of $\underline{h}^{\mathrm{TE}}_{p.t}, \underline{h}^{\mathrm{TM}}_{p\,t}, \underline{h}^{\mathrm{TE}}_{n,t}, \underline{h}^{\mathrm{TM}}_{n,t}$ on the applicators apertures, which are computed easily. Then the infinite summation with respect to m is computed by truncating as high as $m \sim 20$ and the infinite inverse Fourier integral transformation, obtained then, is computed by applying a Gauss rule integration algorithm. A sufficient number of integration points are taken to ensure accuracy. Furthermore the bounds of the integral are truncated as high as $k \sim 30k_0$ to attain good convergence.

By solving the system of linear (37), the expansion coefficients $g_{q,n}$ and $f_{q,n}$ of the field on each waveguide aperture $(q = 1,2,3,4)$ are computed and then the scattering matrix coefficients can be easily obtained.

IV. Numerical Results and Discussion

The effects of coupling between elements of a multi-applicator hyperthermia system are significant in designing and operating this type of systems. In principle, the matching of applicators to independent sources of the same frequency with phase control is a part of an optimization strategy to achieve a desired SAR distribution inside the medium to be heated. In case of using isolators prior to each radiating element, still the coupling phenomena between applicators are important because of the modification of aperture fields through the coupling phenomena. The effect of coupling is expressed by using the scattering matrix notation involving self reflection and mutual coupling coefficients.

TABLE I
Tissue Electrical Parameters at 37°C

	Dielectric constant			Conductivity (S/m)		
Frequency (MHz)	100	433	915	100	433	915
skin	69	47	45	0 62	0.84	0 97
fat	15	15	15	0 22	0 26	0.35
muscle	71 5	57	55 4	0 83	1 12	1 45

The coupling coefficients between elements may be readily computed by exciting one element and computing the amplitude and phase of the TE_{10} mode coefficients coupled to the other waveguide applicators (mutual coupling coefficients) and the coefficient of the reflected TE_{10} mode on the same aperture (self reflection coefficient). The ratio of the induced TE_{10} mode coefficient at ℓth element $(\ell = 1,2,3,4)$ to the excitation TE_{10} coefficient at qth element $(q = 1,2,3,4)$ gives the amplitude and the phase of the coupling coefficient $S_{\ell q}$.

By using the analysis presented in the previous sections, the performance of a four element phased array hyperthermia system has been studied. In order to analyze the strength of the coupling phenomena, the ratios between the mutual coupling to self reflection coefficients are calculated at the operation range for various applicator sizes and settings. Two types of applicators are considered with aperture sizes of $5.8 \times 2.9\ \mathrm{cm}^2$ and $15 \times 10\ \mathrm{cm}^2$. The first applicator is loaded with water $(\varepsilon_w = 80)$ while the relative permittivity of the loading material of the second applicator is $\varepsilon_w = 30$. The numerical values of tissue complex permittivities used in the calculations are defined at the operation range $(1.1f_0 - 1.8f_0, f_0$ being the cutoff frequency of the TE_{10} mode), by using the data compiled from the relevant literature [23], which are shown in Table I.

The small aperture applicators are considered to be placed symmetrically at the periphery of a three-layered cylindrical body with circular cross section 11 cm in diameter and with thicknesses of skin and fat layers $\rho_3 - \rho_2 = 0.5$ cm, $\rho_2 - \rho_1 = 1.0$ cm, respectively, (Fig. 2(a)).

In order to check the developed numerical code, several trials have been performed. In the first place the convergence

$$\sum_{n=1}^{\infty} \begin{pmatrix} K^{11}_{pn,\mathrm{EE}} & K^{11}_{pn,\mathrm{EM}} & K^{12}_{pn,\mathrm{EE}} & K^{12}_{pn,\mathrm{EM}} & K^{13}_{pn,\mathrm{EE}} & K^{13}_{pn,\mathrm{EM}} & K^{14}_{pn,\mathrm{EE}} & K^{14}_{pn,\mathrm{EM}} \\ K^{11}_{pn,\mathrm{ME}} & K^{11}_{pn,\mathrm{MM}} & K^{12}_{pn,\mathrm{ME}} & K^{12}_{pn,\mathrm{MM}} & K^{13}_{pn,\mathrm{EM}} & K^{13}_{pn,\mathrm{MM}} & K^{14}_{pn,\mathrm{EM}} & K^{14}_{pn,\mathrm{MM}} \\ K^{21}_{pn,\mathrm{EE}} & K^{21}_{pn,\mathrm{EM}} & K^{22}_{pn,\mathrm{EE}} & K^{22}_{pn,\mathrm{EM}} & K^{23}_{pn,\mathrm{EE}} & K^{23}_{pn,\mathrm{EM}} & K^{24}_{pn,\mathrm{EE}} & K^{24}_{pn,\mathrm{EM}} \\ K^{21}_{pn,\mathrm{ME}} & K^{21}_{pn,\mathrm{MM}} & K^{22}_{pn,\mathrm{ME}} & K^{22}_{pn,\mathrm{MM}} & K^{23}_{pn,\mathrm{EM}} & K^{23}_{pn,\mathrm{MM}} & K^{24}_{pn,\mathrm{EM}} & K^{24}_{pn,\mathrm{MM}} \\ K^{31}_{pn,\mathrm{EE}} & K^{31}_{pn,\mathrm{EM}} & K^{32}_{pn,\mathrm{EE}} & K^{32}_{pn,\mathrm{EM}} & K^{33}_{pn,\mathrm{EE}} & K^{33}_{pn,\mathrm{EM}} & K^{34}_{pn,\mathrm{EE}} & K^{34}_{pn,\mathrm{EM}} \\ K^{31}_{pn,\mathrm{ME}} & K^{31}_{pn,\mathrm{MM}} & K^{32}_{pn,\mathrm{ME}} & K^{32}_{pn,\mathrm{MM}} & K^{33}_{pn,\mathrm{EM}} & K^{33}_{pn,\mathrm{MM}} & K^{34}_{pn,\mathrm{EM}} & K^{34}_{pn,\mathrm{MM}} \\ K^{41}_{pn,\mathrm{EE}} & K^{41}_{pn,\mathrm{EM}} & K^{42}_{pn,\mathrm{EE}} & K^{42}_{pn,\mathrm{EM}} & K^{43}_{pn,\mathrm{EE}} & K^{43}_{pn,\mathrm{EM}} & K^{44}_{pn,\mathrm{EE}} & K^{44}_{pn,\mathrm{EM}} \\ K^{41}_{pn,\mathrm{ME}} & K^{41}_{pn,\mathrm{MM}} & K^{42}_{pn,\mathrm{ME}} & K^{42}_{pn,\mathrm{MM}} & K^{43}_{pn,\mathrm{EM}} & K^{43}_{pn,\mathrm{MM}} & K^{44}_{pn,\mathrm{EM}} & K^{44}_{pn,\mathrm{MM}} \end{pmatrix} \cdot \begin{pmatrix} g_{1,n} \\ f_{1,n} \\ g_{2,n} \\ f_{2,n} \\ g_{3,n} \\ f_{3,n} \\ g_{4,n} \\ f_{4,n} \end{pmatrix} = \begin{pmatrix} 2A_{1,1}\left(\frac{j\gamma_1}{u_1}\right) \\ 0 \\ 2A_{2,1}\left(\frac{j\gamma_1}{u_1}\right) \\ 0 \\ 2A_{3,1}\left(\frac{j\gamma_1}{u_1}\right) \\ 0 \\ 2A_{4,1}\left(\frac{j\gamma_1}{u_1}\right) \\ 0 \end{pmatrix} \quad (37)$$

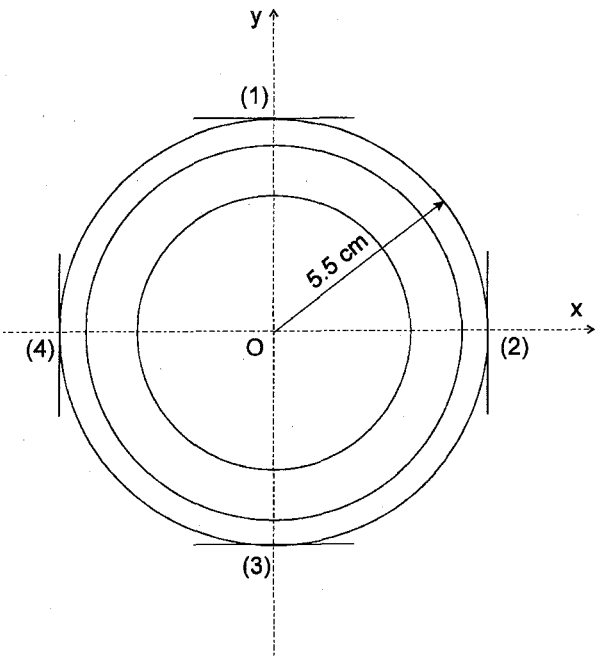

(a)

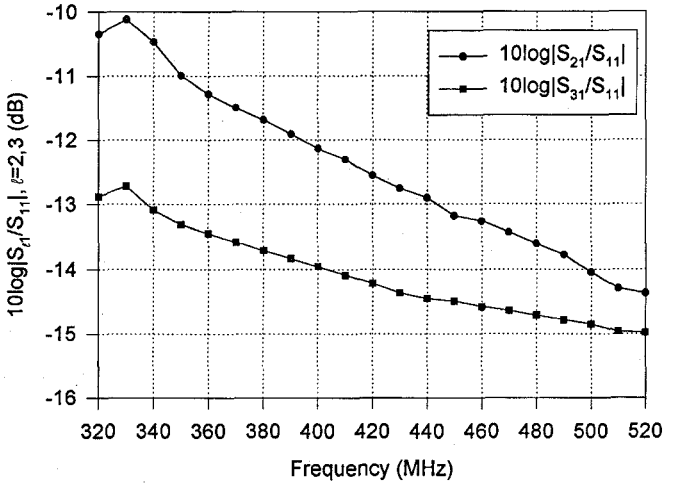

(b)

Fig. 2. (a) Four rectangular aperture (5.8×2.9 cm^2) waveguide applicators placed symmetrically at the periphery of a cylindrical body model of circular cross section, 11 cm in diameter. (b) The ratios in dB of the mutual coupling coefficients $S_{21} = S_{41}$ (between neighboring applicators) and S_{31} (between opposite applicators) to self reflection coefficient (S_{11}), at the operation range of the system.

and stability of the solution are examined by increasing the number of modes included in the aperture electric fields (36). On each applicator aperture a subset of modes are excited. In Table II, convergence patterns are presented in terms of the self reflection coefficient (S_{11}) and the mutual coupling coefficients with neighboring ($S_{21} = S_{31}$) and opposite (S_{41}) applicators, by increasing the number of modes appearing on the excited aperture (1). The remaining parameters of the scattering matrix can be easily obtained by making use of symmetry. Furthermore, the continuity of the tangential fields at the $\rho = \rho_1$ and $\rho = \rho_2$ interface planes has been checked and verified numerically.

In Fig. 2(b), the ratio $|S_{\ell 1}/S_{11}|$ for $\ell = 2, 3, 4$ is presented in dB for the symmetric configuration of Fig. 2(a), while in Fig. 3(b) the same ratios are presented for the configuration shown in Fig. 3(a). In both settings, the coupling between neighboring applicators is stronger compared to distant applicators. In nonsymmetric applicator setting (Fig. 3) strong coupling phenomena (-2.8 dB) are observed at the low frequency edge of the operation bandwidth (low edge $= 1.1 f_0$, f_0 being the cutoff frequency of the TE_{10} mode).

In Fig. 3(c) the ratio $|S_{\ell 2}/S_{22}|$ for $\ell = 1, 3, 4$ is presented in dB for the nonsymmetric setting. For $\ell = 1$, it is observed that the coupling coefficient S_{12} between receiving (1) and transmitting (2) applicators is similar when applicator (1) is excited and applicator (2) is the receiving applicator (coupling coefficient S_{21} (see Fig. 3(b)) as it was expected from reciprocity's principle. Slight differences between $|S_{21}/S_{11}|$ and $|S_{12}/S_{22}|$ shown in Fig. 3(b) and (c), respectively, are due to the difference between the self reflection coefficients S_{11} and S_{22}. The remaining elements of the scattering matrix of the system can be obtained from the coupling coefficients presented in Fig. 3(b) and (c), by making use of the symmetry.

Then, the effect of the target dimensions on the coupling parameters is investigated, by considering a three-layered cylindrical tissue model, 13 cm in diameter (Fig. 4(a)), with skin and fat thicknesses as in the case of Fig. 2(a). The small aperture applicators are assumed to be placed symmetrically at its periphery and the coupling parameters are presented in Fig. 4(b), in the same manner as in Fig. 2(b). The increase in the target dimensions leads into a decrease of the order of 2 dB in the coupling parameters for the entire frequency range. The coupling between opposite applicators still remains weaker compared to neighboring applicators, becoming comparable with the latter at the high frequency edge of the operation bandwidth (high edge $= 1.8 f_0$, f_0 being the cutoff frequency of the TE_{10} mode) and at 335–340 MHz, where a weak resonance phenomenon is observed. At this frequency, power seems to be transmitted to the opposite applicator, resulting in a decrease in the coupling between neighboring applicators and an increase in the coupling between opposite applicators.

Coupling phenomena between large aperture applicators have been also studied as shown in Fig. 5. The waveguide apertures are considered to be symmetrically placed at the periphery of a cylindrical body of circular cross section, 20 cm in diameter. The irradiated body consists of three layers (skin-fat-muscle) with skin and fat thicknesses of 0.5 cm and 1.0 cm, respectively. Phasing phenomena are observed on the fine structure of $|S_{\ell q}|$ scattering parameters. The coupling phenomena between applicators are significantly small compared to small aperture applicators. At high frequencies the coupling between neighboring applicators is of the order of -20 dB while the coupling between the opposite elements is almost independent of frequency (-14 dB). This type of behavior is explained by considering the prevalence of propagation modes of transfer at high frequencies.

Considering the above presented numerical results, it is clear that the magnitude of the coupling is influenced by the frequency and the distance between the elements of the array. Furthermore, the effects of coupling may be significantly

TABLE II
CONVERGENCE FOR THE SELF REFLECTION COEFFICIENT $S_{11} = A'_{1,1}$ (SEE (19)) AND MUTUAL COUPLING COEFFICIENTS WITH NEIGHBORING APPLICATORS $S_{21} = A'_{2,1} = S_{41} = A'_{4,1}$ AND OPPOSITE APPLICATOR $S_{31} = A'_{31}$ FOR THE CONFIGURATION OF FIG. 2(a) AT 433 Mhz, BY INCREASING THE APERTURE MODE NUMBER

Modes appearing on the excited aperture (1)	S_{11}	$S_{21}=S_{41}$	S_{31}
TE_{10}	0.4386 ∠23.3°	0.0223 ∠144.1°	0.01525 ∠17.6°
TE_{10} TE_{12} TM_{12}	0.415 ∠20.5°	0.0215 ∠141.7°	0.0149 ∠15.6°
TE_{10} TE_{12} TE_{30} TE_{32} TM_{12} TM_{32}	0.412 ∠20°	0.0217 ∠141.7°	0.0150 ∠15°

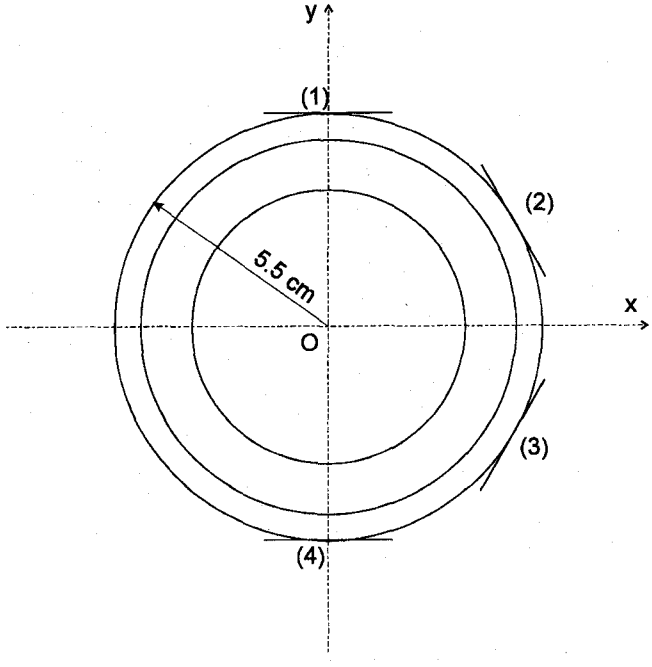

(a)

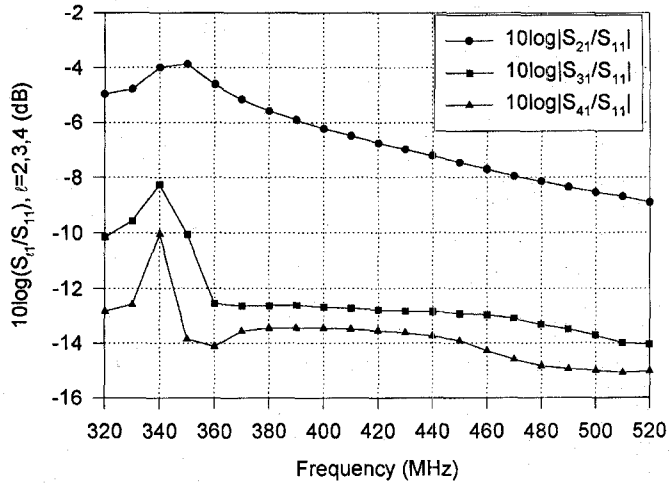

(b)

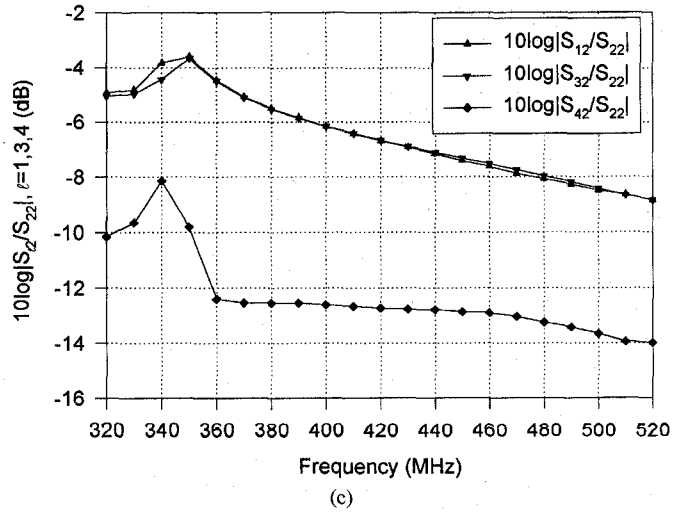

(c)

Fig. 3. (a) Nonsymmetric configuration for the waveguide applicators and the body model of Fig. 2(a). (b) The ratios, in dB, of the mutual coupling coefficients $S_{\ell 1}$ ($\ell = 2, 3, 4$) to self reflection coefficient (S_{11}) of applicator (1), at the operation range of the system. (c) The ratios, in dB, of the mutual coupling coefficients $S_{\ell 2}$ ($\ell = 1, 3, 4$) to self reflection coefficient (S_{22}) of applicator (2), at the operation range of the system.

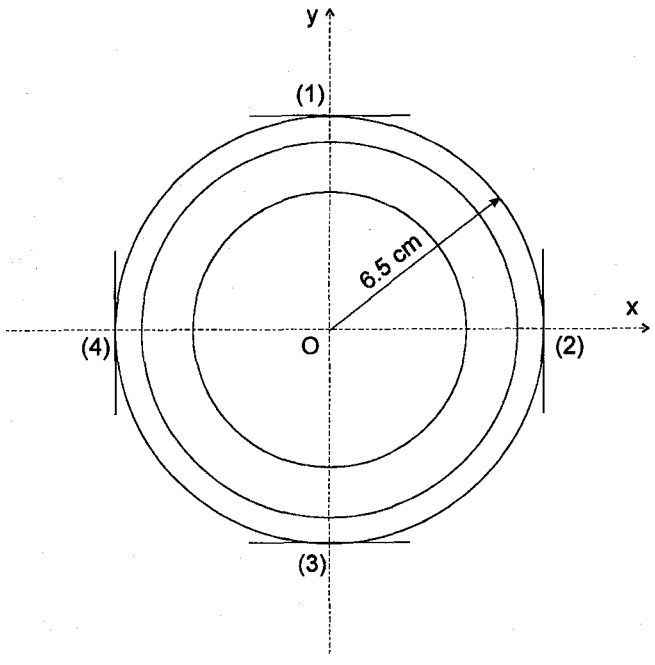

(a)

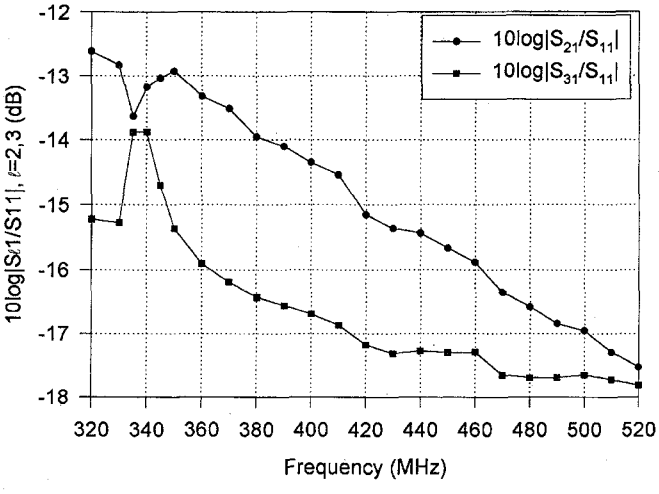

(b)

Fig. 4. (a) Four rectangular aperture (5.8×2.9 cm^2) waveguide applicators placed symmetrically at the periphery of a cylindrical body model of circular cross section, 13 cm in diameter. (b) The ratios in dB of the mutual coupling coefficients $S_{21} = S_{41}$ (between neighboring applicators) and S_{31} (between opposite applicators) to self reflection coefficient (S_{11}), at the operation range of the system.

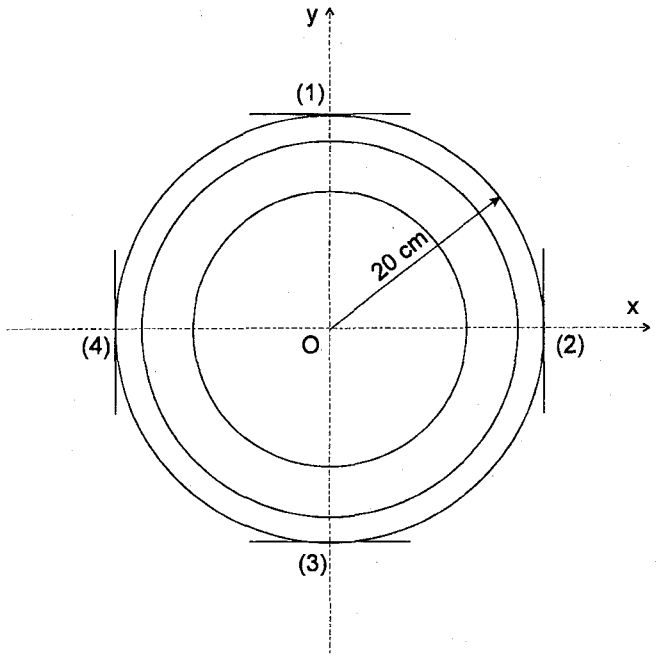

(a)

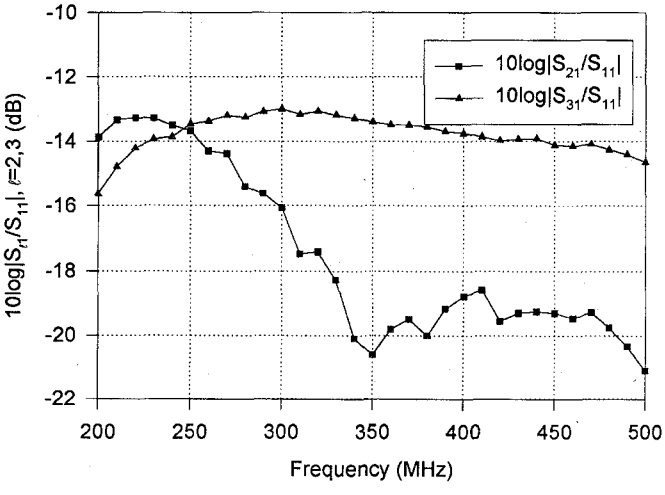

(b)

Fig. 5. (a) Four large aperture ($15\times$ 10 cm^2) waveguide applicators placed symmetrically at the periphery of a three layered cylindrical body model of circular cross section. (b) The ratios, in dB, of the mutual coupling coefficients (between neighboring $(S_{21} = S_{41})$ and opposite (S_{31}) applicators) to the self reflection coefficient (S_{11}), at the operation range of the system.

strong that the impedance of the elements in the array can be drastically altered. In order to achieve in practice a stable operation of each waveguide applicator and a good match to a power generator, the strength of the coupling appearing between the applicators of the system must be estimated. In addition, the modification of the field distribution at each aperture, caused by the other applicators is of great interest in hyperthermia applications, since the field on each aperture must be known with high precision in order to achieve a desired power distribution inside the body. A four applicator-element phased array hyperthermia system has been developed [7] and the analysis presented in this paper is being employed to compute and optimize the power patterns inside tissues. The developed optimization algorithm will be presented elsewhere.

It is important to emphasize that in the presented numerical results all boundary conditions are satisfied on the interfaces between tissue layers (exactly) and on the waveguide apertures (approximately in a point matching sense). Considering also the fact that the field expressions satisfy Maxwell's equations, it is concluded that the presented results are self-consistent and accurate within the framework of the approximate solution of the system of integral equations (33).

V. Conclusion

A semianalytical solution has been presented for the power coupling between the waveguide applicators of a phased array hyperthermia system radiating into a three-layered cylindrical tissue model of circular cross section. Scattering parameters indicating the effect of coupling via the radiating apertures of a four element phased array hyperthermia system have been computed for two alternative practical waveguide applicators of 5.8×2.9 cm^2 and 15×10 cm^2 aperture size. These results are useful in designing and operating phased array hyperthermia systems and in estimating and optimizing the deposited power distribution inside tissues.

Appendix

A. Kernel Matrix Functions $\underline{\bar{K}}_{\ell q}(x, y/x', y')$

$$\underline{\bar{K}}_{\ell q}(x, y/x', y') = \int_{-\infty}^{+\infty} dk \sum_{m=-\infty}^{+\infty} e^{jm(\varphi_{0\ell}-\varphi_{0q})} e^{jm\left(-\frac{x}{\rho_3}+\frac{x'}{\rho_3}\right)} \times e^{jk(y-y')} \underline{\bar{N}}(m,k) - \delta_{\ell q} \underline{\bar{\Omega}}(x, y/x', y') \quad (\ell = 1,2,3,4; q = 1,2,3,4) \tag{A1}$$

where

$$\underline{\bar{N}}(m,k) = \frac{1}{(2\pi)^2} \frac{jk_3}{\omega\mu_0\mu_3\rho_3} \underline{\bar{L}}'(m,k;\rho_3)(\underline{\bar{L}}(m,k;\rho_3))^{-1} \tag{A2}$$

where

$$\underline{\bar{L}}'(m,k;\rho_3) = \underline{\bar{T}}_{3m}^{(1)}(k;\rho_3) + \frac{Y_m(\alpha_3\rho_3)}{J_m(\alpha_3\rho_3)} \underline{\bar{T}}_{3m}^{(2)}(k;\rho_3))^{-1} \underline{\bar{R}}_{3m} \tag{A3}$$

$$\underline{\bar{\Omega}}(x, y/x', y') = \sum_{n=1}^{\infty} \left\{ \left(-\frac{\gamma_n}{\omega\mu_0\mu_w} \right) \underline{h}_{n,t}^{\mathrm{TE}} \underline{e}_{n,t}^{\mathrm{TE}} + \left(\frac{\omega\varepsilon_0\varepsilon_w}{\lambda_n} \right) \underline{h}_{n,t}^{\mathrm{TM}} \underline{h}_{n,t}^{\mathrm{TM}} \right\} \tag{A4}$$

and $\delta_{\ell q}$ is the Kronecker's delta.

References

[1] G. Arcangeli, P. P. Lombardini, G. A. Lovisolo, G. Marsiglia, and M. Piatelli, "Focusing of 915 MHz electromagnetic power on deep human tissues," *IEEE Trans. Biomed. Eng.*, vol. BME-31, pp. 47–52, 1984.

[2] J. W. Hand, J. L. Cheetham, and A. J. Hind, "Absorbed power distribution from coherent microwave arrays for localized hyperthermia," *IEEE Trans. Microwave Theory Tech.*, vol. MTT-34, pp. 484–489, 1986.

[3] P. F. Turner, "Mini annular phased array for limb hyperthermia," *IEEE Trans. Microwave Theory Tech.*, vol. MTT-34, pp. 508–513, 1986.

[4] E. J. Gross, T. C. Cetas, P. R. Stauffer, R. W. Liu, and M. L. D. Lumori, "Experimental assessment of phased array heating of neck tumors," *Int. J. Hyperthermia*, vol. 6, pp. 453–474, 1990.

[5] P. F. Turner *et al.*, "Future trends in heating technology of deep seated tumors," in *Application of Hyperthermia In Treatment of Cancer*, vol. 107, R. D. Issels and W. Wilmans, Eds. Berlin: Springer-Verlag, 1987, pp. 249–262.

[6] J. D. P. Van Dijk, C. Schneider, R. Van Os, L. Blank, and D. Gonzalez, "Results of deep body hyperthermia with large waveguide radiators," in *Consensus on Hyperthermia for the 1990's*, H. I. Bicher *et al.*, Eds. New York: Plenum, 1990, pp. 315–320.

[7] N. K. Uzunoglu, K. S. Nikita, and N. G. Maratos, "Four element computer controlled 432 MHz phased array hyperthermia system," in *Consensus on Hyperthermia for the 1990's*, H. I. Bicher *et al.*, Eds., New York: Plenum, 1990, pp. 311–314.

[8] V. Sathiaseehan, M. F. Iskander, G. C. Howard, and N. M. Bleehan, "Theoretical analysis and clinical demonstration of the effect of power pattern control using the annular phased array hyperthermia system," *IEEE Trans. Microwave Theory Tech.*, vol. MTT-34, pp. 514-519, 1986.

[9] J. T. Loane and S. W. Lee, "Gain optimization of a near field focusing array for hyperthermia applications," *IEEE Trans. Microwave Theory Tech.*, vol. 37, pp. 1629–1635, 1989.

[10] A. Boag, Y. Leviatan, and A. Boag, "Analysis and optimization of waveguide multiapplicator hyperthermia systems," *IEEE Trans. Biomed. Eng.*, vol. 40, pp. 946–952, 1993.

[11] K. S. Nikita, N. G. Maratos, and N. K. Uzunoglu, "Optimal steady-state temperature distribution for a phased array hyperthermia system," *IEEE Trans. Biomed. Eng.*, vol. 40, pp. 1299–1306, 1993.

[12] J. Chen and O. P. Gandhi, "Numerical simulation of annular phased arrays of dipoles for hyperthermia of deep seated tumors," *IEEE Trans. Biomed. Eng.*, vol. BME-39, pp. 209–216, 1992.

[13] K. D. Paulsen, J. W. Strohbehn, and D. R. Lynch, "Theoretical electric field distributions produced by three types of regional hyperthermia devices in a three-dimensional homogeneous model of man," *IEEE Trans. Biomed. Eng.*, vol. 35, pp. 36–45, 1988.

[14] R. J. Myerson, L. Leybovich, B. Emami, P. W. Grigsby, W. Straube, and D. Von Gerichten, "Phantom studies and preliminary clinical experience with the BSD 2000," *Int. J. Hyperthermia*, vol. 7, pp. 937–951, 1991.

[15] P. F. Turner *et al.*, "Steerable phased arrays for hyperthermia," in *Proc. 9th Annual Conf. IEEE-EMBS, IEEE Service Center*, pp. 1326–1328, 1987.

[16] C. J. Schneider and J. D. P. Van Dijk, "Visualisation by a matrix of emitting diodes of interference effects from a radiative four-applicator hyperthermia system," *Int. J. Hyperthermia*, vol. 7, pp. 355–366, 1991.

[17] L. B. Leybovich, R. J. Myerson, B. Emami, and W. L. Straube, "Evaluation of the sigma 60 applicator for regional hyperthermia in terms of scattering parameters," *Int. J. Hyperthermia*, vol. 7, pp. 917–935, 1991.

[18] V. Teodoridis, T. Sphicopoulos, and F. Gardiol, "The reflection from an open-ended rectangular waveguide terminated by a layered dielectric medium," *IEEE Trans. Microwave Theory Tech.*, vol. MTT-33, pp. 359–372, 1985.

[19] K. S. Nikita and N. K. Uzunoglu, "Analysis of the power coupling from a waveguide hyperthermia applicator into a three layered tissue model," *IEEE Trans. Microwave Theory Tech.*, vol. 37, pp. 1794-1801, 1989.

[20] R. Antolini, G. Cerri, L. Christoferetti, and R. De Leo, "Absorbed power distributions from single or multiple waveguide applicators during microwave hyperthermia," *Phys. Med. Biol.*, vol. 31, pp. 1005–1019, 1986.

[21] J. A. Stratton, *Electromagnetic Theory*. New York: McGraw-Hill, 1941.

[22] D. S. Jones, *Theory of Electromagnetism*. Oxford: Pergamon Press, 1964, Ch. 5, pp. 248–251.

[23] H. P. Schwan and K. R. Foster, "RF field interactions with biological systems: Electrical properties and biophysical mechanism," in *Proc. IEEE*, 1980, vol. 68, pp. 104–113.

Konstantina S. Nikita was born in Tripoli, Greece, in 1963. She received the Diploma in electrical engineering and the Ph.D. degree from the National Technical University of Athens, Greece, in 1986 and 1990, respectively. She received the M.D. degree from the University of Athens, Greece, in 1993.

Since 1990, she has been working as a Researcher at the Institute of Communication and Computer Systems, National Technical University of Athens, Greece. Recently, she has been elected Assistant Professor at the Department of Electrical and Computer Engineering, National Technical University of Athens. Her current research interests include applications of electromagnetic waves in medicine, clinical application of hyperthermia, electromagnetic scattering, nonlinear optimization algorithms and applications.

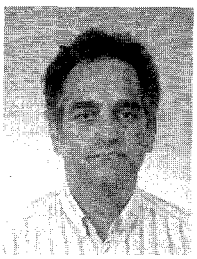

Nikolaos K. Uzunoglu (M'82) was born in Constantinopole, Turkey, in 1951. He received the B.Sc. degree in electronics from the Technical University of Istanbul in 1973 and the M.Sc. and Ph.D. degrees in 1974 and 1976, respectively, from the University of Essex, England.

He worked from 1977 to 1984 as a Research Scientist at the Office of Research and Technology of the Hellenic Navy. In 1984, he was elected Associate Professor at the National Technical University of Athens, Department of Electrical Engineering, and in 1987 he was promoted to Professor. In 1986 he was elected Vice Chairman of the Department of Electrical Engineering of the National Technical University of Athens, and in 1988 he was elected Chairman of the same Department. He was reelected as Chairman in 1990 and 1992 twice. In 1991, he was elected and appointed Director of the Institute of Communication and Computer Systems, an independent research establishment associated with the National Technical University of Athens. His research interests include electromagnetic scattering, propagation of electromagnetic waves, fiber optics telecommunications, and high-speed circuits operating at gigabit/second rates. He has 90 publications in refereed international journals, and he has published three books in Greek on microwaves, fiber optics telecommunications and radar systems.

In 1981, Dr. Uzunoglu received the International G. Marconi Award in Telecommunications. Since 1988 he has been the National Representative of Greece to the COST, Technical Telecommunications Committee, actively participating in several COST telecommunications projects. Further, he has been Project Manager of several RACE, ESPRIT, and National Research and Development Projects in the fields of telecommunications and biomedical engineering applications.